Eur Biophys J (2011) 40:131–141
DOI 10.1007/s00249-010-0631-x

ORIGINAL PAPER

Development of fluorophore dynamics imaging as a probe for lipid domains in model vesicles and cell membranes

Stanley W. Botchway · Amanda M. Lewis · Christopher D. Stubbs

Received: 25 June 2010 / Revised: 27 September 2010 / Accepted: 28 September 2010 / Published online: 15 October 2010

Abstract The ability to detect raft structures in membranes continues to present a problem, especially in the membranes of live cells. Rafts, generally considered to be small (<200 nm) sphingolipid-rich regions, are commonly modelled using lipid vesicle systems where the ability of fluorophore-labelled lipids to preferentially locate into domains (basically large rafts) is investigated. Instead, in this study the *motional* properties of different fluorophores were determined using two-photon excitation and time-correlated single-photon counting coupled with diffraction-limited imaging with polarizing optics in scanning mode to obtain nanosecond rotational correlation time images. To develop the method, well-characterized domain-containing models consisting of giant unilamellar vesicles comprising mixtures of 1-palmitoyl-2-oleoyl-*sn*-glycero-3-phosphocholine, sphingomyelin and cholesterol were used with the fluorophores diphenylhexatriene, 1-palmitoyl-2-{6-[(7-nitro-2-1,3-benzoxadiazol-4-yl)amino]hexanoyl}-*sn*-glycero-3-phosphocholine and 1,2-dioleoyl-*sn*-glycero-3-phosphoethanolamine-*N*-(7-nitro-2-1,3-benzoxadiazol-4-yl). Accordingly, images of rotational correlation times of the probes revealed domain structures for all three probes consistent with other studies using different approaches. Rotational correlation time images of living cell membranes were also observed. The method has the advantage that not only does it enable domains to be visualised or imaged in a unique manner but that it can also potentially provide useful information on the lipid dynamics within the structures.

S. W. Botchway · A. M. Lewis · C. D. Stubbs (✉)
Lasers for Science, Central Laser Facility,
Science and Technology Facilities Council,
Rutherford Appleton Laboratory,
Harwell Science and Innovation Campus,
Didcot OX11 0QX, UK
e-mail: chris.stubbs@stfc.ac.uk

Keywords Domains · Rafts · Fluorescence anisotropy imaging · Lipid dynamics · Lipid vesicles · DPH · NBD · Multiphoton excitation

Abbreviations

NBD-PC	1,2-Dioleoyl-*sn*-glycero-3-phosphoethanolamine-*N*-(7-nitro-2-1,3-benzoxadiazol-4-yl) (ammonium salt)
POPC	1-Palmitoyl-2-oleoyl-*sn*-glycero-3-phosphocholine
NBD-PE	1-Palmitoyl-2-{6-[(7-nitro-2-1,3-benzoxadiazol-4-yl)amino]hexanoyl}-*sn*-glycero-3-phosphocholine
DPH	1,6-Diphenyl-1,3,5-hexatriene

Introduction

The idea of rafts (Simons and Ikonen 1997) provided an immediately attractive hypothesis for organisational entities in membranes acting as platforms for signalling complexes in cells. This has led to a plethora of investigations of model raft systems in lipid vesicles and many attempts to observe the structures in cell membranes, the latter with varying success (Silvius 2005; Duggan et al. 2008; Pike 2009). There has been some controversy in agreeing on the size and nature of rafts in the field, leading to a recent attempt at a standard definition that membrane rafts are small (10–200 nm), heterogeneous, highly dynamic, sterol- and sphingolipid-enriched domains that compartmentalize cellular processes. Small rafts can sometimes be stabilized to form larger platforms through protein–protein and protein–lipid interactions (Pike 2006). However, even this

definition still does not address issues of the lifetime of the rafts and the dynamics of their lipid components, and also since rafts are intrinsically dynamic structures to a great extent, the method for observing the rafts in a real sense defines the raft itself. Whether the raft as physically observed coincides in a relevant manner with a functionally definable system does not necessarily follow. It should be pointed out that the literature has yet to fully adopt the above definition of a raft, and the term "rafts" has hereto been applied to structures of all sizes; here we use the term "raft" ($\sim$<200 nm) as a subset of the term "domain", covering structures of any size. Many studies, including the present, utilize model systems of simple lipid mixtures to develop techniques for domain investigation and to learn more about the behaviour of these entities. In such studies it is important to recognise that the structures in the model system may only mimic those in cell membranes, especially when it comes to size.

Due to the resolution limit imposed by the wavelength of light there has been some discussion as to the ability of these approaches to detect such structures in more complex cell systems where the rafts may be quite small. There is also the problem that, when it comes to cell membranes, rafts may exist for very short times, requiring short data collection times; consequently, there is an ever-increasing demand for improved detector sensitivity. With newer, high-resolution optical technologies currently emerging, it is likely that the spatial resolution and temporal limitations will soon be overcome (Duggan et al. 2008). Most of the approaches using fluorescence probes rely on the probe partitioning differently into rafts and non-raft regions, the intensity and lifetime property then being determined or imaged. Although these methods have proved useful, excited-state lifetimes tend to be relatively insensitive to differing lipid compositions such as are encountered in raft compared with non-raft regions. We considered that, by contrast to the lifetime, lipid probe dynamics would vary by as much as an order of magnitude, potentially facilitating the visualisation of domains in general and in addition yielding information about the structures in question.

Using relatively simple model systems usually based on giant unilamellar lipid vesicles (GUVs), which provide an ideal system (Wesolowska et al. 2009), and phosphatidylcholine/cholesterol/sphingomyelin mixtures, the basic features of lipid-based domain structures have been established in numerous investigations. Fluorescence microscopy lends itself to the examination of raft or domain structures in model systems, with most investigations using probes that locate differently into domain and non-domain regions (de Almeida et al. 2009); for example, fluorescence lifetime imaging (Margineanu et al. 2007; Haluska et al. 2008; Stockl et al. 2008), fluorescence energy transfer (Loura et al. 2009) and fluorescence correlation spectroscopy (Kahya et al. 2004; Ariola et al. 2009) have all been used to examine raft-like structures. Cholesterol, being a key raft component, has been used in the form of bodipy-cholesterol to study cholesterol interactions and dynamics in the form of rotational diffusion, bulk time-resolved anisotropy and steady-state polarization imaging (Ariola et al. 2009); this is one of very few studies aimed at not just identifying the raft/domain but also obtaining information on lipid dynamics.

Here the dynamics of fluorescent lipid probes co-dispersed with lipids as GUVs was investigated to determine if time-resolved fluorescence anisotropy microscopy imaging could be used to probe both domain and non-domain lipid dynamics simultaneously. GUV systems provide a useful model for more complex cell membranes, and many studies have aimed to identify domains in these structures using a variety of methods; thus, it was possible to prepare GUVs that, based on the literature, are known to contain domains or raft-like structures and which could then be used to study lipid probe dynamics as a method for revealing the structures.

We postulated that fluorescent probes might experience different dynamics as a reflection of local lipid composition in different domain regions. To accomplish this we used probes of the different regions of the lipid bilayer including DPH, and NBD-lipids with the NBD group on the acyl chain or the head group region. For this a confocal multi-photon excitation microscopy approach was developed using polarizing optics. The lipids used were chosen specifically to test the procedure because they have been well studied before and in mixtures known to produce non-random mixing in the form of domain structures. The results show that the dynamics of lipid probes can indeed be used to distinguish such regions in model membranes. Initial explorations of cell membranes reveal similar structures.

Materials and methods

POPC, DOPC, NBD-PC and NBD-PE were from Avanti Polar Lipids. DPH, Sphingomyelin (brain) and cholesterol were from Sigma Chem. Co. All other chemicals used were of analytical grade. MCF-7 cells were a kind gift from Dr. Brenda Twomey (UCB Celltech, UK) and were cultured in DMEM/F12 medium supplemented with 10% foetal calf serum, in 3-ml glass-bottom dishes (supplemented with 100 units/ml penicillin, 100 μg/ml streptomycin and 2 mM L-glutamine).

Vesicle preparation

GUVs were prepared by the electroformation method (Angelova and Dimitrov 1988). An appropriate mixture of lipid and probe in chloroform was deposited onto two parallel platinum wires, and the solvent was evaporated under nitrogen. The assembly was suspended in a chamber and subjected to an alternating current (AC) frequency of 10 Hz with voltage increasing from 0.2 to 1 V. The basic set-up is illustrated in Fig. 1a, b, the vesicle chamber being placed on the stage of an inverted Nikon TE2000-U fluorescence microscope. The vesicles grew on the wires over 0–2 h and were stable for several hours (Fig. 1c). Using this method it is generally assumed that unilamellar vesicles are obtained, although it is possible that multilayers might also exist; however, the bilayers would be essentially independent, so that this would not have any significant bearing on the experiments.

Fluorescence imaging

The source of excitation was a titanium sapphire mode-locked laser tunable between wavelengths of 700 and 980 nm, running at 75 MHz with 180 ps pulses (Mira 900F, Coherent), delivered to the microscope stage via a custom-built *x*–*y* galvanometer scanner as illustrated in Fig. 2. The laser and half-wave plate were tuned to a wavelength suitable for two-photon excitation of the fluorophore to be used, and the half-wave plate was set to vertically polarize the laser light. The vertically polarized and focussed laser light was then scanned across the sample. Fluorescence intensities of the polarization components parallel and perpendicular to that of the laser were simultaneously collected and separated by a polarizing beam splitter (99.5% reflecting) and simultaneously detected by a Becker and Hickl multichannel photomultiplier tube (PML-16-C) as shown in Fig. 3a. This development was essential mainly because even slight vesicle movement with time was unavoidable and it also avoids other errors that might result from collecting vertical and horizontal images by re-scanning the same region sequentially. The data from the PML-16-C, galvanometer scanning mirrors and laser pulse rate were processed by a personal computer (PC), and fluorescence decay curves for the two channels were assembled on a pixel-by-pixel basis. These data were processed by imaging software which allowed χ^2 values for the fluorescence decay curves to be assessed for goodness of fit. The data were analysed using custom-made software (OptiSpec; Becker and Hickl, GmbH) to calculate the fluorescence anisotropy at each pixel and at each point in time, fitting generated images of rotational correlation time etc. as required, allowing all parameters to run free.

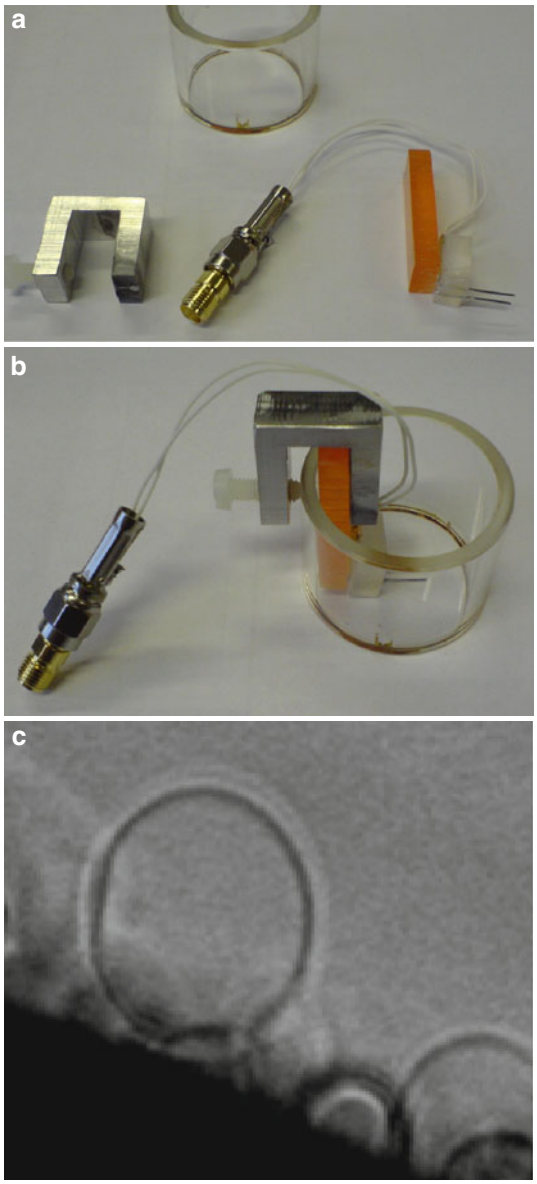

Fig. 1 **a**, **b** GUV chamber: In the assembled chamber the platinum wires rested on a coverslip, and the lipid and probe mixture in chloroform was deposited onto the wires, evaporated by a stream of nitrogen, then phosphate-buffered saline pH 7.4 was added and an AC current of 10 Hz applied, as described in the "Materials and methods" section. **c** Photograph of a POPC GUV on the platinum wire

Data were analysed according to $r(t)$, the anisotropy decay with time, given by

$$r(t) = \frac{I_{VV}(t) - GI_{VH}(t)}{I_{VV}(t) + 2GI_{VH}(t)}, \quad (1)$$

where I is the intensity of emission observed through vertically (V) or horizontally (H) oriented polarizers upon excitation with vertically polarized light (I_{VV} and I_{VH}). G is given by I_{HV}/I_{HH}, the ratio of the emission intensities with excitation with horizontally orientated polarized light

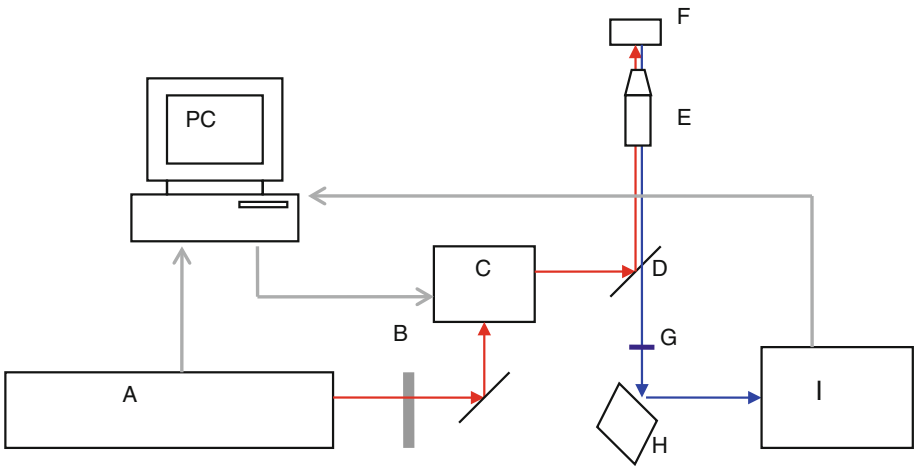

Fig. 2 Diagram showing the basic layout used for anisotropy imaging. A: Coherent Mira 900F 180-fs 80-MHz pulsed titanium sapphire mode-locked laser, tunable between 700 and 950 nm. B: Half-wave plate tunable to operate between 150 and 6,000 nm (Alphalas), used for controlling the polarization of the excitation light and measuring the *G*-factor. C: Computer-controlled galvanometric scanning mirror system scans the laser spot across a region of interest within the sample, typically 75 μm × 75 μm. D: Dichroic reflecting laser light between 680 and 1,000 nm and transmitting fluorescence below 650 nm. E: Objective lens, 60×/1.2 Plan Apo VC (Nikon), focusses laser onto sample. F: Sample position. G: BG39 transmission filter (Comar) to prevent scattered and reflected laser light from being detected. H: Prism reflecting fluorescence onto detection equipment. I: Detection equipment position

observed through vertically (V) or horizontally (H) oriented polarizers.

For a hindered rotator, $r(t)$ is given by

$$r(t) = (r_0 - r_\infty)\mathrm{e}^{-t/\phi} + r_\infty, \quad (2)$$

where r_0 is the anisotropy of the fluorophore in the absence of depolarizing motion, r_∞ is the value to which the anisotropy decays for times longer than the fluorescence lifetime (zero for free rotator, non-zero for a hindered rotator) and ϕ is the rotational correlation time. When analysing the data on a pixel-by-pixel basis for imaging purposes, in practice, the signal-to-noise ratio is such that a reasonable approximation can be made assuming $r_\infty = 0$. However, when binning numbers of pixels together and analysing according to the above equation, it was clear that r_∞ was zero for NBD-PE but not for DPH and NBD-PC. Thus the imaging data recovered gives only an approximate ϕ value. This, however, does not prevent the analysis from being used to reveal inhomogeneities, such as would be represented by domains.

Results and discussion

Using the electroformation method, large (<5 to 50 μm) vesicles were found to grow in stable fashion on the platinum wires. When intensity images of GUVs were collected they showed a systematic asymmetric distribution of intensity, as previously reported using steady-state polarization video microscopy (Florine-Casteel 1990), and this was found for all probes examined (Fig. 3b). This was due to the nature of the incident light (being polarized) only exciting those fluorophores that are appropriately aligned (discussed further below).

To analyse the time-resolved anisotropy, two approaches were initially used. The simultaneous polarization emission I_{VH} and I_{VH} images were collected, and the image data were analysed by various rotational models, including a single rotational correlation time, a single rotational correlation time plus r_∞ or two rotational correlation times, with a single fluorescence lifetime, accomplished by binning nine pixels together using Origin graph analysis software. The best fit was to either of the later models; however, using the Becker and Hickl custom software, only the single rotational correlation time model was available. Since they were limited to analysis of only a single pixel, using the latter two models would not have proven more reliable in terms of χ^2. Thus, for the purpose of comparing the different bilayer compositions, the pixel-by-pixel imaging mode analysis provided by the Becker and Hickl software was used. Thus, while the actual rotational correlation time values are model dependent and therefore approximations, what is important is the *variation* in the different bilayer regions, which is model independent.

For DPH in POPC GUVs the top of the vesicle (Fig. 4), corresponding to the vertical frame of reference, the rotational correlation times were short, on the order of 2 ns. By contrast, for values on the sides of the vesicle, horizontal to the frame of reference, the majority of the region showed correlation times of 10–20 ns. This can be rationalised on the basis of the diagram shown in Fig. 5, where based on the literature (Barrow and Lentz 1985; Florine-Casteel

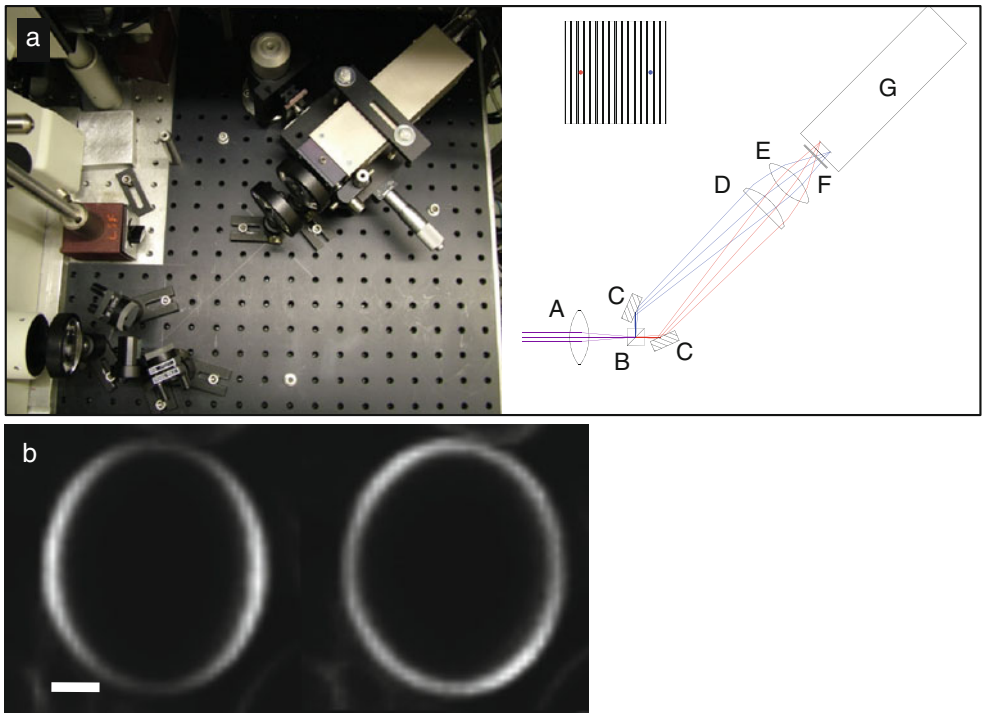

Fig. 3 **a** V-format set-up, showing the paths taken by horizontally polarized light (shown in *red*, travelling straight through the cube) and vertically polarized light (shown in *blue*, reflected through 90° by the cube). The light fluoresced by the sample has negligible divergence as it exits the microscope. A: Lens 1, f60 UV fused silica 50-mm-diameter bi-convex lens. B: Cube polarizer 16 JP 01 (Comar), positioned with its beam-splitting plane at the focal plane of lens 1. C: Semrock MM1-311S-25.0 MaxMirrors, mounted at 66° to the closest face of the cube polarizer. D: Lens 2, f100 UV fused silica 50-mm-diameter bi-convex lens. E: Lens 3, f50 UV fused silica 50-mm-diameter bi-convex lens. F: BG39 bandpass filter, which transmits less than 1% of light between 700 and 950 nm, and so prevents laser reflections from being detected. G: PML-16-C (Becker and Hickl GmbH), 16-channel photomultiplier tube, mounted on micrometer-controlled stages allowing positional control, connected to an SPCM 830 PCI card and used with SPCM software (all Becker and Hickl GmbH). Also shown is a diagram of the photomultiplier tube (PMT) array, with *red* and *blue spots* (not to scale) representing the positions of the focussed horizontally and vertically polarized light. *Inset* diagram of the PMT array. **b** Light intensity image taken through the system with vertically polarized excitation observed through vertically (*left*) and horizontally (*right*) oriented polarizers (I_{VV}, $_{VH}$). (*bar* 1 μm)

1990), two subpopulations of DPH are known to exist at any one moment, although they will exchange freely. One is located in the bilayer centre, and the other is between acyl chains, thus excitation with polarized light selects the former at the vesicle top/bottom but the latter (more restricted/slower motion) at the vesicle sides, the motion being more restricted for the latter. The DPH can probe from the bilayer centre (less restricted) to near the head group region (most restricted) and to regions in between, resulting in a range of correlation times rather than two distinct correlation times. The lifetime showed two centres corresponding to the two regions, but it was not sensitive enough to provide information on domains. The unique aspect of this method of detecting regions such as domains is that other methods depend on the probes locating within these regions, introducing a limitation, whereas here the known ability of DPH to be present in all regions (with largely invariant lifetime) means it is the motion of the probe that betrays the existence of a lipid domains and that only when the motion (as distinct from the lifetime) is examined do these regions become visible.

Addition of cholesterol with POPC caused increased rotational correlation times, in keeping with the results of previous studies showing an ordering effect (Straume and Litman 1987) (see Table 1). The results for POPC/cholesterol/sphingomyelin (1:1:1 molar ratio) are shown in Fig. 6 and are summarised in Table 1 where it can be seen that, apart from a dramatic increase in the rotational correlation time, there is a great deal of heterogeneity along the vesicle sides (although it is actually all round the vesicle, it is only seen here due to the polarization optics) with distinct regions on the order of 1–2 μm in size. This illustrates the main aim of the work, i.e. to use a system known to produce domains or raft-mimicking structures to determine whether anisotropy imaging can be used to detect and study such features. From numerous papers in the literature, the presence of sphingomyelin and cholesterol with POPC results in domain structures (mimicking rafts),

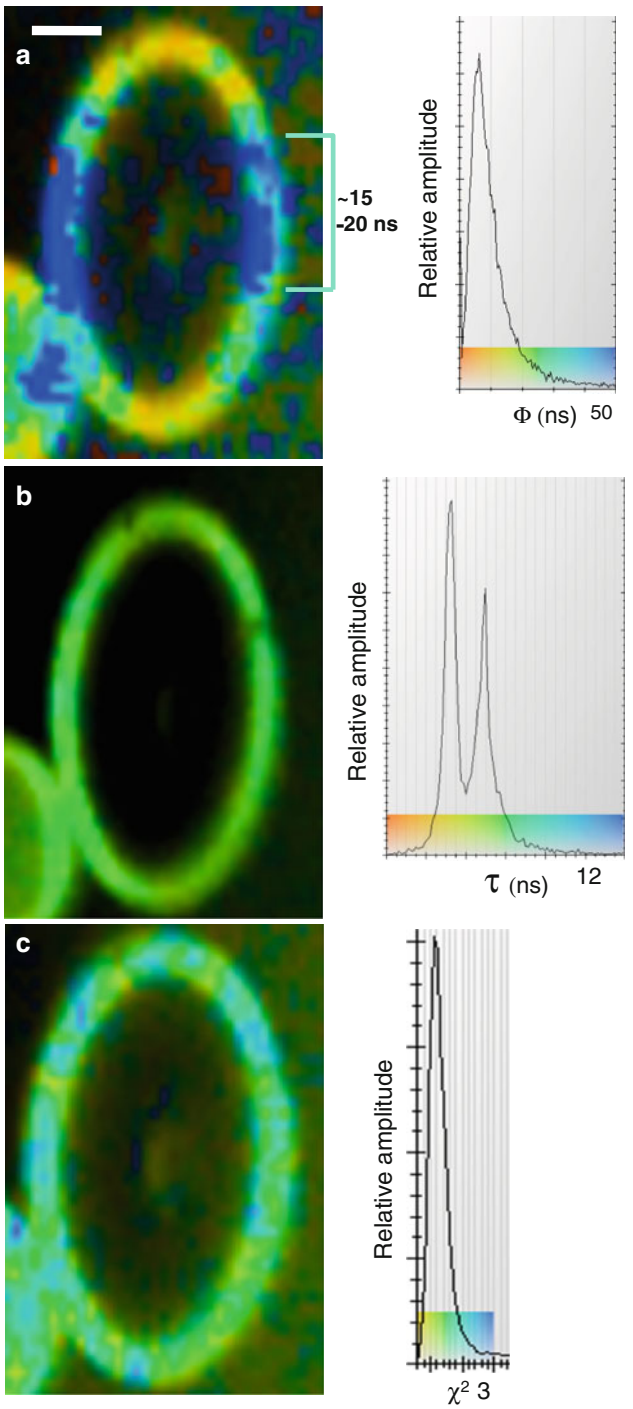

Fig. 4 POPC GUV images labelled with DPH (0.25 mol%) (*left*). **a** Rotational correlation time image (*left*) and respective colour coding (*right*). **b** Lifetime image (*left*) and respective colour coding (*right*). (**c**) χ^2 image (*left*) and respective colour coding (*right*). (*bar* 1 μm)

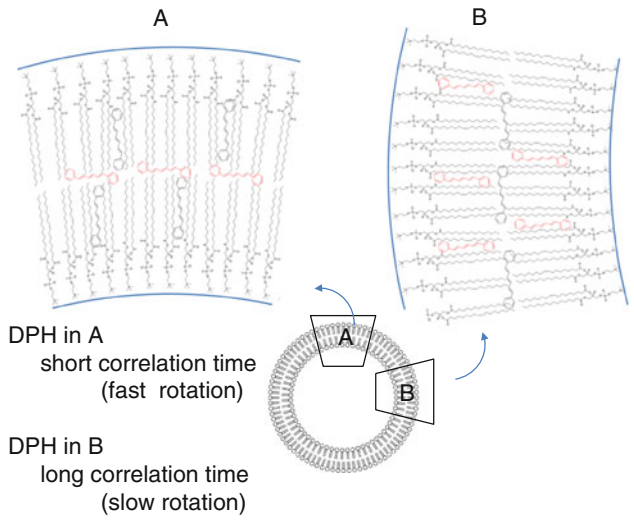

Fig. 5 Diagram showing the orientations of DPH that are excited to produce fluorescence by photo-selection according to the polarization direction at the top and sides of a POPC vesicle (shown in *red*). DPH is known to locate both in the centre of the bilayer and also between the acyl chains. Thus, rotational correlation times for the top and sides of the vesicle will represent the motions in these two distinct regions. (for POPC)

and we are able to detect these as regions of differing probe motion.

DPH is known to locate in all membrane regions, in keeping with the observations here (Lentz 1989; Florine-Casteel 1990; de Almeida et al. 2003). Along the vesicle sides, only DPH that is aligned with the acyl chains can be excited to fluoresce and therefore be observed and is either in a domain enriched with cholesterol and sphingomyelin and is exhibiting slower motion or is in a non-domain POPC-enriched region (faster motion). This effect is reinforced by the distribution of DPH between the bilayer centre and between acyl chains, increasing in the latter as a function of the presence of cholesterol (Straume and Litman 1987). The DPH that is located in the bilayer *centre* does not appear to have an appreciably different motion in the domain compared with non-domain regions, since there was no observable motional heterogeneity at the vesicle top/bottom (Fig. 7). Of course, the DPH may adopt intermediate confirmations, so two discrete correlation times will not be observed but rather a continuum between the two locations.

The images collected for the rotational correlation time of NBD-PC in POPC, cholesterol, sphingomyelin (1:1:1) mixed vesicles reveal domains with slower lipid motion seen along the vesicle sides, similar to the situation with DPH (Fig. 8). In Table 1, as for DPH, addition of cholesterol and sphingomyelin causes a decreased rotational correlation time, observable along the vesicles side and as increased heterogeneity due to domain formation. However, the explanation of how the domain and non-domain regions are visualised is slightly different, and here the NBD-PC in the domains would appear to possess a different *configuration* than in the non-domain regions. The

Table 1 Comparison of the analysis of DPH fluorescence decay on a pixel-by-pixel basis using Optispec software ("calculated") compared with analysis of groups of nine binned pixels analysed using Origin graph analysis software ("image data"), showing reasonable agreement for POPC GUV. Summary data for GUV with cholesterol and with cholesterol and sphingomyelin are also shown

	POPC Calculated[1]	POPC Image data[2]	POPC/cholesterol (3:1) Image data[2]	POPC/cholesterol/sphingomyelin (1:1:1) Image data[2]
ϕ(ns)				
Vesicle top/bottom				
DPH	1.4 (±0.31)	2.0	15	2.8
NBD-PC	–	5	0.7–1	1.2
NBD-PE		~0.5–1	–	~1
Vesicle sides				
DPH	22.8 (±2.5)	10–50	10–70	10–300
NBD-PC	–	~1	10–20	7 to >50
NBD-PE		3–8	–	15–30

[1] Data analysed using Origin graph software on binned pixels

[2] Data taken from images analysed using Optispec software

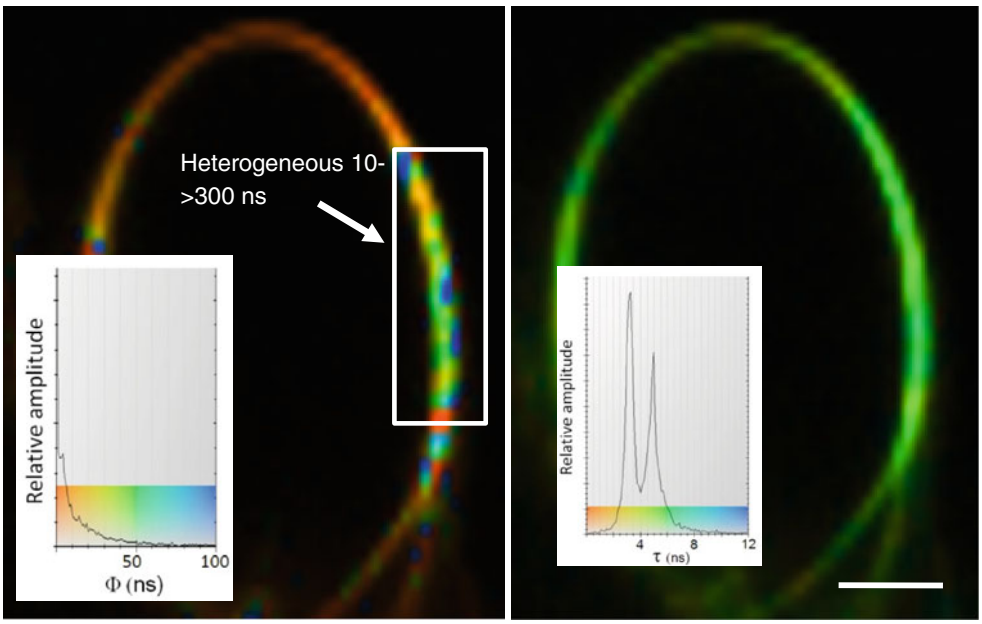

Fig. 6 Rotational correlation time image (*left*) and lifetime image (*right*) of a representative GUV consisting of POPC, cholesterol, sphingomyelin (1:1:1 molar ratio) labelled with DPH (0.25 mol%) (*inset graphs* show colour coding). *Insets*: colour-coded graph showing the distribution of rotational correlation times/lifetimes for the image. The colour coding shows areas with 0–100 ns correlation time, although single-point analysis revealed areas with regions up to ~300 ns. (*bar* 1 μm)

NBD chromophore at the end of the 6-acyl chain is known to be able to curve up and locate under the head group region (Chattopadhyay and London 1987; Huster et al. 2001; Loura and Ramalho 2007). This indicates that the domain structures with their more restricted environment could contain NBD-PC with a straightened-out acyl chain, thus restricting the NBD group and its motion, as shown in Fig. 9. These structures are not seen at the vesicle top/bottom due to the orientation of the NBD in these regions being unfavourable for excitation. By contrast, the NBD chromophores in the non-domain areas would be expected to be more randomly organised, so that some of the non-domain probe population in both the vesicle sides and top/bottom are oriented favourably for excitation, the resultant correlation time being relatively short as expected. The results obtained here are in broad agreement with a recent imaging study that used the fluorescence lifetime of NBD-PC to detect "rafts" (Stockl et al. 2008); however, the narrow range of lifetimes covering domain and non-domain areas compared with the much larger range of

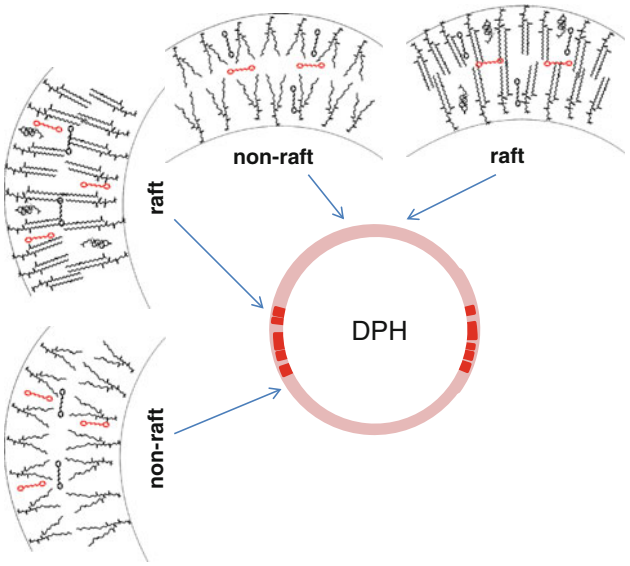

Fig. 7 Diagram showing proposed orientations of DPH that are excited to produce fluorescence by photo-selection according to polarization direction at the top and sides of a POPC, cholesterol, sphingomyelin (1:1:1, molar) vesicle (shown in *red*). Top/bottom: only DPH in the bilayer centre contributes fluorescence; sides: only DPH sitting between the acyl chains contributes fluorescence. Note that, in this model, DPH motion is the same in the domain and non-domain areas at the top/bottom, so domain areas are not distinguishable on the basis of DPH motion, in contrast with the vesicle sides

rotational correlation times we observe suggests that our method may be more sensitive in domain detection as well as potentially providing more information on the different domain environments. Indeed in the lifetime study they suggest that there was a small, high-lifetime "raft" component not always discernible in the images but only apparent in the overall analyses.

In domains the NBD of NBD-PC is constricted and aligned such that it can only be excited by the polarized light when at the vesicle sides, but non-domain NBD is disoriented and can be seen all round the vesicle. This accounts for the more even distribution of intensity observed through vertical and horizontally oriented polarizers for NBD-PC as compared with DPH.

In a previous time-resolved anisotropy study it was observed that the time-resolved anisotropy of the NBD of NBD-PE in DOPC bilayers decayed to zero (Greiner et al. 2009), indicating that the NBD was acting as an unhindered rotor (i.e. zero r_∞), a result we also found here (analysis not shown) and contrasting with the case with the situation with DPH and the NBD of NBD-PC, which are both hindered rotators due to the positioning in the acyl chain region. The NBD of NBD-PE is at the bilayer surface, which means that it has no preferential orientation with reference to the polarization direction when lying on the vesicle surface (Fig. 10e, direction B); by contrast, when angled as far from the vesicle surface as possible, it would have an alignment that is so-oriented (Fig. 10e, direction A). The lifetime data show a shorter lifetime for the top/bottom of the NBD-PE-labelled GUV and a corresponding shorter correlation time (Fig. 10a, c). By contrast, at the vesicle sides, the NBD that is excited to fluoresce is lying in the surface, where it experiences a more restricted freedom of motion. The observation of domain structures on the GUV sides suggests that the NBD (of NBD-PE) is only restricted in domain structures relative to non-domain areas when it is lying on the bilayer surface.

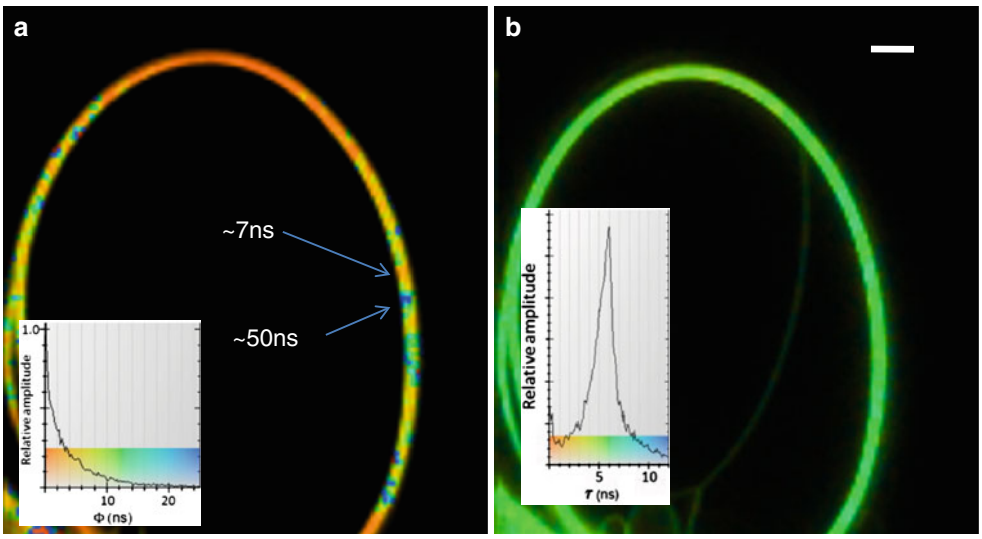

Fig. 8 Rotational correlation time image **a** and lifetime image **b** of a representative GUV consisting of POPC, cholesterol, sphingomyelin (1:1:1) labelled with NBD-PC (1 mol%). *Insets*: colour coded graphs showing the distribution of rotational correlation times/lifetimes for the entire image. (*bar* 10 μm)

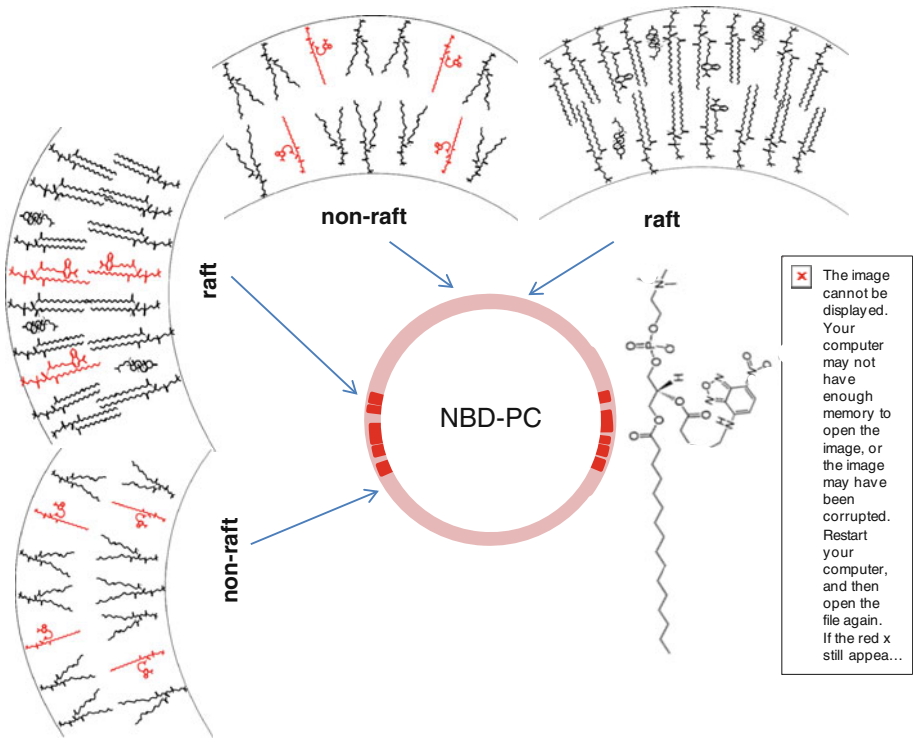

Fig. 9 Diagram showing the proposed orientations of the NBD moiety in NBD-PC. In this case the NBD can orient either near the head group region or between the acyl chains. In this interpretation the domain areas accommodate the latter, which are only excited to fluoresce at the vesicle sides, whereas NBD located at the head group region (non-domain location) would be randomly oriented and so always excited

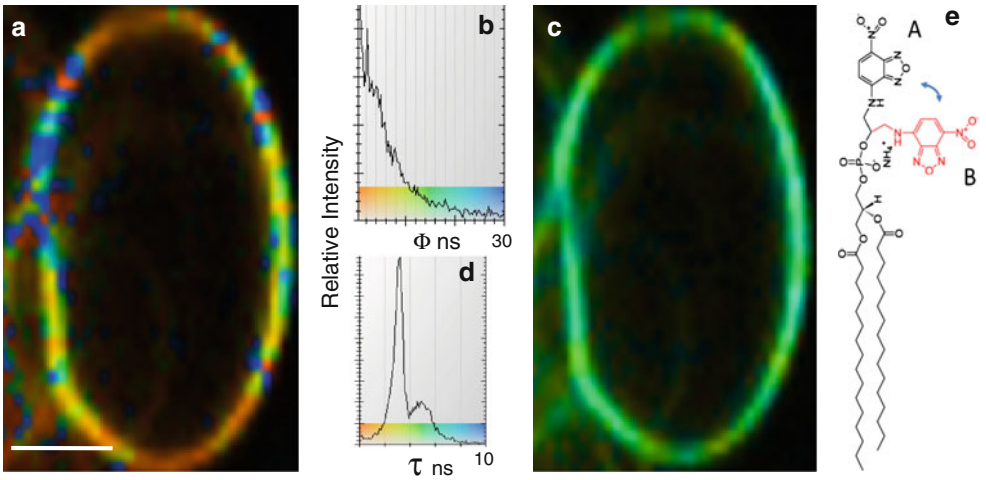

Fig. 10 Rotational correlation time image **a** and lifetime image **b** of a representative GUV consisting of POPC, cholesterol, sphingomyelin (1:1:1) labelled with NBD-PE (1 mol%) with respective colour coded graphs representing the entire image (**b**, **d**), and diagram showing the orientations of the NBD group available to the NBD of NBD-PE. (*bar* 1 μm)

Finally, we obtained a rotational correlation time image for NBD-PC dispersed into the membranes of living MCF-7 cells (Fig. 11). After addition of NBD-PC, the outer membrane is labelled and a heterogeneous distribution of rotational correlation times is apparent. This indicates that this approach has the potential to study domain structures in cell membranes, and also rafts. Clearly the nature and indeed existence of rafts (i.e. domains of <200 nm size) remains an unresolved issue in the literature. However, cell membranes also have much larger areas of interest in the membrane, for example cell leading edges, caps, areas involved in endocytosis, various vesicles inside the cell with different lipid/protein compositions etc., which may all be classified as domains and which could all potentially be studied by this approach.

In this work domains were visualised by means of time-resolved fluorescence anisotropy imaging of GUVs using DPH and NBD-PC and NBD-PE. The domains varied in size in the ~0.5 to 1+ μm range and were stable, at least over the time period of the measurement, which was 1–2 min. However, regarding the size of domains in POPC/cholesterol/sphingomyelin mixtures, elsewhere it has been

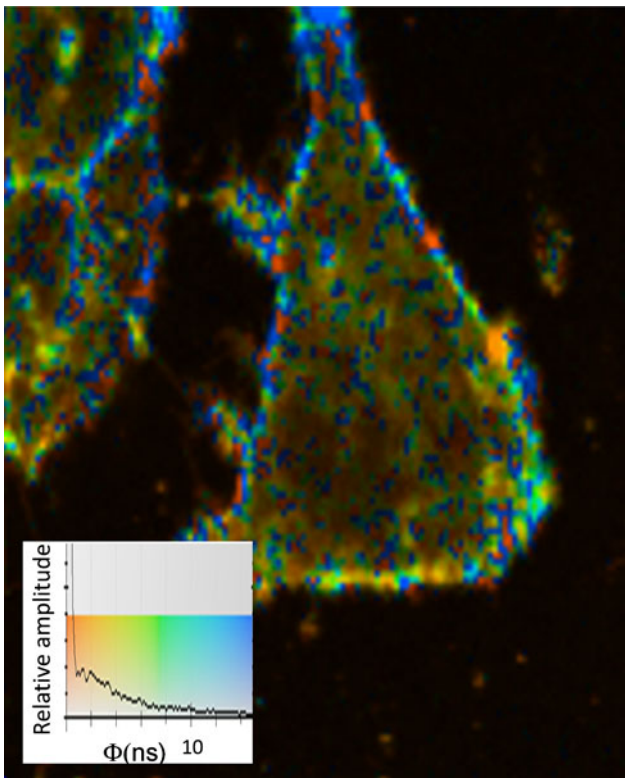

Fig. 11 Rotational correlation time image of MCF-7 cells labelled with NBD-PC (after 40 min). The chloroform from 100 nmole NBD-PC was evaporated under nitrogen, and 100 μL buffer was added, followed by vortexing. NBD-PC suspension (10 μL) was added to the cells in serum-free media (MEM) in a glass-bottom 2-mL Petri dish and mixed before examination at various time periods under the microscope. The image shown was collected after 40 min exposure to the NBD-PC; *inset* is colour-coded distribution of the rotational correlation time over the entire image

stated that they may range from as small as 20 nm to several hundred nanometres across (although this is highly dependent on the working definition of the raft/domain, since they are likely to be transient structures) (Hwang et al. 1998; Silvius 2003; de Almeida et al. 2005; Frazier et al. 2007). With super-resolution techniques (~20 nm) such as stimulated emission depletion (STED) or stochastic optical reconstruction (STORM) combined with the anisotropy imaging technique as described herein it should be possible to observe raft structures directly.

Acknowledgments We are grateful to Dr. Axel Bergman of Becker & Hickl GmbH for help with the analysis, to Prof. Tony Parker for help and support, and to the Lasers for Science Facility (CLF, STFC Rutherford Appleton laboratory) for access.

References

Angelova MI, Dimitrov DS (1988) A mechanism of liposome electroformation. Prog Colloid Polym Sci 76:59–67

Ariola FS, Li Z, Cornejo C, Bittman R, Heikal AA (2009) Membrane fluidity and lipid order in ternary giant unilamellar vesicles using a new bodipy-cholesterol derivative. Biophys J 96:2696–2708

Barrow DA, Lentz BR (1985) Membrane structural domains. Resolution limits using diphenylhexatriene fluorescence decay. Biophys J 48:221–234

Chattopadhyay A, London E (1987) Parallax method for direct measurement of membrane penetration depth utilizing fluorescence quenching by spin-labeled phospholipids. Biochemistry 26:39–45

de Almeida RF, Fedorov A, Prieto M (2003) Sphingomyelin/phosphatidylcholine/cholesterol phase diagram: boundaries and composition of lipid rafts. Biophys J 85:2406–2416

de Almeida RF, Loura LM, Fedorov A, Prieto M (2005) Lipid rafts have different sizes depending on membrane composition: a time-resolved fluorescence resonance energy transfer study. J Mol Biol 346:1109–1120

de Almeida RF, Loura LM, Prieto M (2009) Membrane lipid domains and rafts: current applications of fluorescence lifetime spectroscopy and imaging. Chem Phys Lipids 157:61–77

Duggan J, Jamal G, Tilley M, Davis B, McKenzie G, Vere K, Somekh MG, O'Shea P, Harris H (2008) Functional imaging of microdomains in cell membranes. Eur Biophys J 37:1279–1289

Florine-Casteel K (1990) Phospholipid order in gel- and fluid-phase cell-size liposomes measured by digitized video fluorescence polarization microscopy. Biophys J 57:1199–1215

Frazier ML, Wright JR, Pokorny A, Almeida PF (2007) Investigation of domain formation in sphingomyelin/cholesterol/POPC mixtures by fluorescence resonance energy transfer and Monte Carlo simulations. Biophys J 92:2422–2433

Greiner AJ, Pillman HA, Worden RM, Blanchard GJ, Ofoli RY (2009) Effect of hydrogen bonding on the rotational and translational dynamics of a headgroup-bound chromophore in bilayer lipid membranes. J Phys Chem B 113:13263–13268

Haluska CK, Schroder AP, Didier P, Heissler D, Duportail G, Mely Y, Marques CM (2008) Combining fluorescence lifetime and polarization microscopy to discriminate phase separated domains in giant unilamellar vesicles. Biophys J 95:5737–5747

Huster D, Muller P, Arnold K, Herrmann A (2001) Dynamics of membrane penetration of the fluorescent 7-nitrobenz-2-oxa-1, 3-diazol-4-yl (NBD) group attached to an acyl chain of phosphatidylcholine. Biophys J 80:822–831

Hwang J, Gheber LA, Margolis L, Edidin M (1998) Domains in cell plasma membranes investigated by near-field scanning optical microscopy. Biophys J 74:2184–2190

Kahya N, Scherfeld D, Bacia K, Schwille P (2004) Lipid domain formation and dynamics in giant unilamellar vesicles explored by fluorescence correlation spectroscopy. J Struct Biol 147:77–89

Lentz BR (1989) Membrane fluidity as detected by diphenylhexatriene probes. Chem Phys Lipids 50:171–190

Loura LM, Ramalho JP (2007) Location and dynamics of acyl chain NBD-labeled phosphatidylcholine (NBD-PC) in DPPC bilayers. A molecular dynamics and time-resolved fluorescence anisotropy study. Biochim Biophys Acta 1768:467–478

Loura LM, de Almeida RF, Silva LC, Prieto M (2009) FRET analysis of domain formation and properties in complex membrane systems. Biochim Biophys Acta 1788:209–224

Margineanu A, Hotta J, Vallee RA, Van der Auweraer M, Ameloot M, Stefan A, Beljonne D, Engelborghs Y, Herrmann A, Mullen K, De Schryver FC, Hofkens J (2007) Visualization of membrane rafts using a perylene monoimide derivative and fluorescence lifetime imaging. Biophys J 93:2877–2891

Pike LJ (2006) Rafts defined: a report on the Keystone symposium on lipid rafts and cell function. J Lipid Res 47:1597–1598

Pike LJ (2009) The challenge of lipid rafts. J Lipid Res 50(Suppl): S323–S328

Silvius JR (2003) Fluorescence energy transfer reveals microdomain formation at physiological temperatures in lipid mixtures modeling the outer leaflet of the plasma membrane. Biophys J 85:1034–1045

Silvius J (2005) Lipid microdomains in model and biological membranes: how strong are the connections? Q Rev Biophys 38:373–383

Simons K, Ikonen E (1997) Functional rafts in cell membranes. Nature 387:569–572

Stockl M, Plazzo AP, Korte T, Herrmann A (2008) Detection of lipid domains in model and cell membranes by fluorescence lifetime imaging microscopy of fluorescent lipid analogues. J Biol Chem 283:30828–30837

Straume M, Litman BJ (1987) Influence of cholesterol on equilibrium and dynamic bilayer structure of unsaturated acyl chain phosphatidylcholine vesicles as determined from higher order analysis of fluorescence anisotropy decay. Biochemistry 26:5121–5126

Wesolowska O, Michalak K, Maniewska J, Hendrich AB (2009) Giant unilamellar vesicles—a perfect tool to visualize phase separation and lipid rafts in model systems. Acta Biochim Pol 56:33–39